

Spreading of Carbopol Gels

D. D. Pelot¹, N. Klep², A. L. Yarin^{*1,3}

¹Department of Mechanical and Industrial Engineering, University of Illinois at Chicago, 842 W. Taylor St., Chicago IL 60607-7022, U.S.A.

²Department of Material Science and Engineering, Clemson University, 161 Surrine Hall, Clemson, SC, 29634, U.S.A.

³College of Engineering, Korea University, Seoul, S. Korea

Abstract

This work aims to study flows within a wedge at the inclination angles in the 5°-20° range. Flow within a wedge occurs when a Carbopol solution is pulled horizontally by a moving conveyer belt through the wedge apex opening at different speeds. The upper side of the wedge is fixed at the exit by a pivot joint about which it could rotate. At the wedge entrance a force gauge is placed so that it is pushing at the upper side of the wedge to keep it at a predetermined position (and thus at a predetermined inclination angle). The gauge measures the restraining force required to counteract the pressure build-up on the flowing Carbopol solution side and to keep the upper side of the wedge at its position. Visualization through the transparent vertical sides of the wedge was used to track seeding particles inside the solution to reconstruct the velocity profile, and in particular to reveal rigid-like stagnation zones characteristic of the yield-stress liquids.

Introduction

The spreading of soft materials between non-parallel plates is a widely encountered phenomenon, such as spreading of creams, lotions, foods, and construction materials. More specifically, many construction materials are hand-applied using a type of spreading knife: hawk and trowel, application knife, or a draw down bar. Understanding the flow field and forces within the wedge geometry helps companies design the material so that it yields during application but is un-yielded while the material is adjacent to the application tool. During the application of soft materials, sensory feedback is one of the major factors determined by the arising stresses. The spreading process is similar, in a sense, to a journal bearing or screw extruder and therefore can be considered as a lubrication-like process. Then the lubrication approximation can be used in many cases as a powerful tool to describe spreading behavior (Schlichting 1987; Tichy 1991; Weinstein and Ruschak 2004; Tadmor and Gogos 2006).

The approach to soft materials employing the Newtonian fluid model in the lubrication approximation has its advantages and disadvantages. As stated by Wienstein and Ruschak (2004), the major advantage of this approach is that it leads to the one-dimensional Reynolds lubrication equation and allows for a straightforward calculation of the flow field for a given geometry. Even though the pressure distribution is one-dimensional (depends only on the longitudinal coordinate), the velocity profile is two-dimensional, which is accounted for in the framework of this approach. Notably, the Newtonian fluid model is capable of predicting the reverse flow arising due to the adverse (positive) pressure gradient emerging when fluid is pulled under the wedge by its moving bottom side.

However, soft materials, such as those mentioned above, possess a yield stress which might influence their flow when they are spread on a stationary plate by another moving inclined plate, or effectively, flowing inside a wedge. It should be emphasized that in the present article we take the latter point of view, i.e. always consider flows as the flows inside a wedge with an inclined upper side and moving lower side pulling fluid under the wedge. It was shown experimentally by Milne (1954) that stagnation zones arise in specific areas at a certain eccentricity inside a journal bearing containing a Bingham yield-stress fluid. Stagnation zones, or core formation, in lubrication processes have been shown to occur when the pressure gradient is positive (adverse), or as the film thickness increases in the vertical direction, or as the velocity decreases, or any combination of these (Wada et al. 1973). Wada et al. (1973) and Tichy (1991) identified theoretically different types of cores and the conditions necessary for their creation, namely, an attached core or a floating core. An attached core is defined as a plug with uniform velocity equal to that of the moving boundary it is attached to. A floating core is a plug that exists between two domains of flow, for example in the central part of a pipe flow of a Bingham yield-stress fluid (Loitsyanskii 1996).

Modeling using a Bingham yield-stress fluid model for flows inside wedge geometry has also revealed advantages and disadvantages. Similarly to the Newtonian fluid model, the Bingham fluid model can also predict reverse flow velocities under the wedge, but in distinction from the former, the latter can also predict core formation. For a Newtonian fluid, the flow profile is sketched in Fig. 1. This sketch shows the reverse flow arising due to the adverse pressure gradient. If the fluid has a yield stress, such as a Bingham fluid, the flow profile in the reverse flow region would be the most affected.

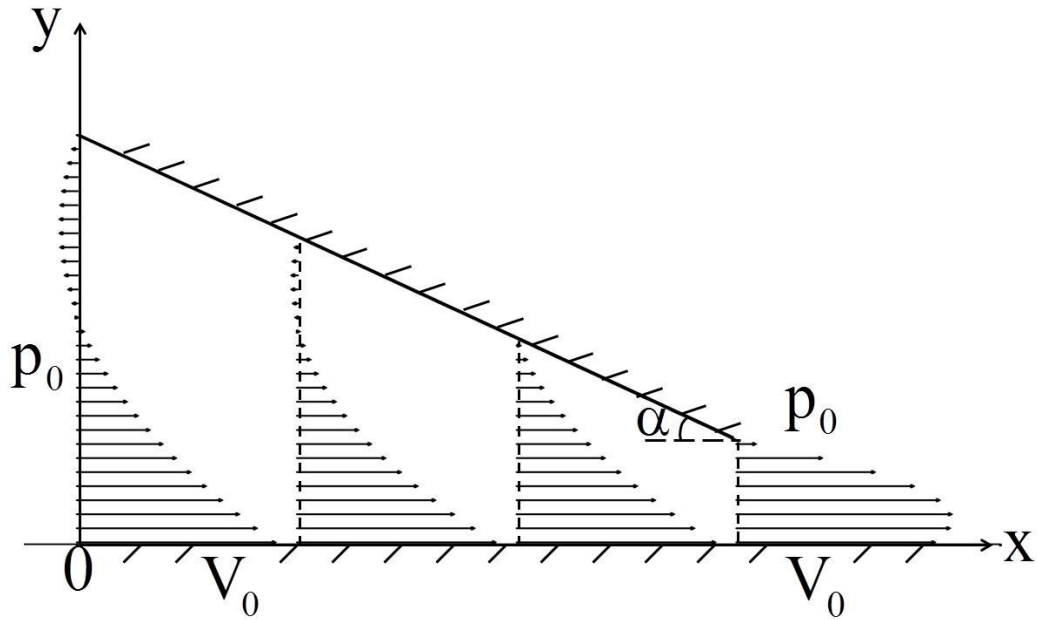


Fig. 1. Velocity profile of a flow within a wedge with an inclination angle α . The atmospheric pressure at the entrance and exit is p_0 . The x axis coincides with the moving bottom side of the wedge, which pulls fluid under it with velocity V_0 .

The modified Reynold equation obtained in the framework of the Bingham fluid model in the cases with or without floating or attached cores does not allow for an easy analytical analysis of the force acting on the inclined upper side of the wedge (Tichy 1991). Other authors have used other analyses or assumptions to determine the velocity field inside a flat wedge-like domain characteristic of spreading. For example, Dorier and Tichy (1992) expressed the viscosity profile of the fluid as a function of a stress parameter loosely related to the yield stress and a strain-rate parameter. If the strain-rate parameter tends to infinity, a Newtonian viscosity is recovered. On the other hand, if the parameter tends to zero, the viscosity increases dramatically representative of a Bingham fluid. Batra (1966), who only considered attached cores, divided the journal

bearing flow into three distinct domains following Milne's (1954) analysis of core formation as a result of the interplay between the pressure gradient, plug height, and the yield stress. Wada et al. (1973) were only able to establish an implicit Reynolds equation.

Plug flows within a yield stress fluid have been recently reviewed by Balmforth et al. (2014). The review shows that the lubrication theory of the yield-stress fluids is an important open issue and many attempts to numerically model a Bingham fluid in eccentric cylinder geometry have been made (Szabo and Hassager 1992; Frigaard and Ryan 2004; Putz et al. 2009).

The aim of the present work is to experimentally examine flows of Carbopol solutions within wedge geometries utilizing different inclination angles and different entrance to exit height ratios, and thus to procure the velocity profiles and the other flow characteristics of a yield-stress fluid moving within a wedge. The experimental velocity profiles are then compared to the theoretical velocity profiles for a Newtonian fluid (Schlichting 1987) and Bingham fluid (Tichy 1991). Next, the effective viscosity of the fluid is calculated using the measured force, moment, and wedge geometry and compared to the rheological parameters found using a rheometer with parallel plate geometry. A Carbopol solution is used in this experiment because it is known to be a yield stress fluid, mimics the soft solids mentioned above, and is ideal for particle image velocimetry (Pelot et al. 2013). The rheological parameters were measured using parallel-plate rheometer with rough and smooth plates and approximately the same results were found. This is an indication that the no-slip condition held in the present case on smooth plates, and the results for the latter are included. Moreover, in Pelot et al. (2013), flow near the boundaries was visualized during viscosity measurements. It was shown that the no-slip boundary condition holds up to the shear rates of the order of 100 1/s. Shear rates greater than 100 1/s were not employed. Similar materials were used in the spreading experiments.

The experimental material, setup and image analysis method are described in detail in the Experimental materials and methods section. The experimental results are presented versus the predictions of the Newtonian and Bingham models in the Results section. A discussion of the results is in the Discussion section. Conclusions are then drawn.

Experimental materials and apparatus

Material preparation

A 1.5% Carbopol-940 (Lubrizol) aqueous solution was prepared following the manufacturer (Noveon Inc.) specifications. First, 30 g of Carbopol powder was dissolved in 1970 mL of water. The Carbopol was slowly added to water, while stirring on a hotplate at 50 °C, with a magnetic stirrer set to the highest sustainable setting. The solution was allowed stirring overnight. The acidic Carbopol solution was neutralized by slowly adding 1 M NaOH to the required amount specified by the manufacturer. This process created a gel with a yield stress in shear of 570 ± 94 Pa (based on the four measurements shown in Fig. 2b), found using the squeezing apparatus described in Pelot et al. (2013). The squeeze-flow experiments were driven by a constant squeezing force applied to compress a cylindrically-shaped material between two large parallel plates. It should be emphasized that, as usual, the yield stress in shear is found as the yield stress in compression divided by $\sqrt{3}$. Using a TA Instruments HR rheometer with parallel plate geometry (smooth plates), the power-law pseudoplastic rheological behavior in shear flow with the exponent (the behavior index) n and the consistency index K were measured as $n = 0.16$ and $K = 154 \text{ Pa} \times \text{s}^n$ [note that these parameters were found using the Weissenberg-

Rabinowitsch correction, since the shear rate in the radial direction within the parallel plate geometry is not constant, [te Nijenhuis (2007) and Schramm (2000)]. During the measurement the gap size was 1 mm and the test was conducted using a logarithmic shear rate ramp from 1 1/s to 200 1/s. These shear rates are representative of those found in the experiments. The rheological parameters are shown in Fig. 2.

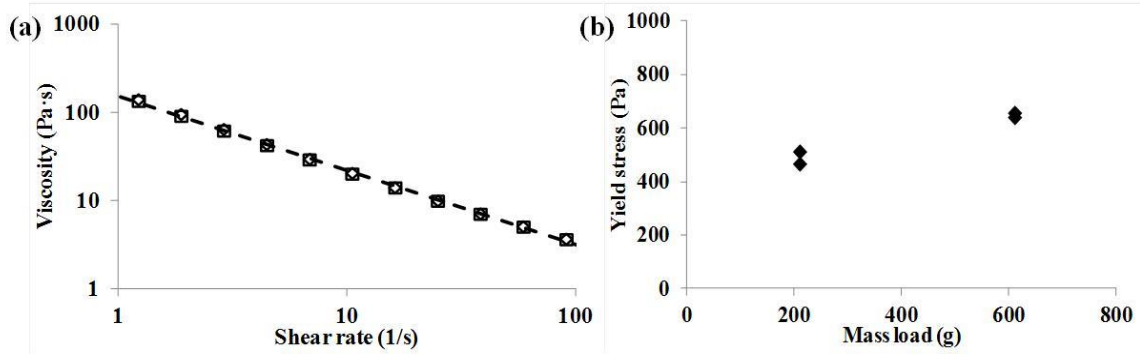


Fig. 2. (a) Viscosity of Carbopol 940 during the shear rate ramp-up (open circles) and shear rate ramp-down (open squares) found using a parallel plate viscometer with smooth plates. (b) Yield stress, τ_0 , for different mass loads measured using the squeezing apparatus. The dashed line was drawn using the fitted rheological parameters mentioned in the text.

Experimental procedure

In the experimental setup shown in Fig. 3 a layer of Carbopol gel was transported on the lower surface moving to the right, while the inclined spreading plate was stationary. The spreading plate was made of acrylic which was 15 cm long, 10 cm wide, and 0.95 cm thick. The moving lower surface was an “infinitely” long polystyrene sheet. It was pulled at different velocities by an AC motor (Leeson M1145033). The force gauge, Imada DS2-11, was connected

to a fixed stand and was always strictly perpendicular to the inclined plate at any inclination. Due to the Carbopol gel pressure, it could partially escape from the wedge-like gap sidewise. To prevent such deviations from the two-dimensional flow, vertical walls were fixed on both sides of the wedge.

The preliminary experiments on Carbopol spreading revealed that bubbles inevitably entrapped inside the gel may serve as seeding particles. However, it was found that washed coffee blended in the Carbopol gel are better seeding particles because of their size commensurate with the image resolution. They are also preferable given their availability, contrast, and non-hazardous nature. The images with these seeding particles being visible are shown in Fig. 3(b).

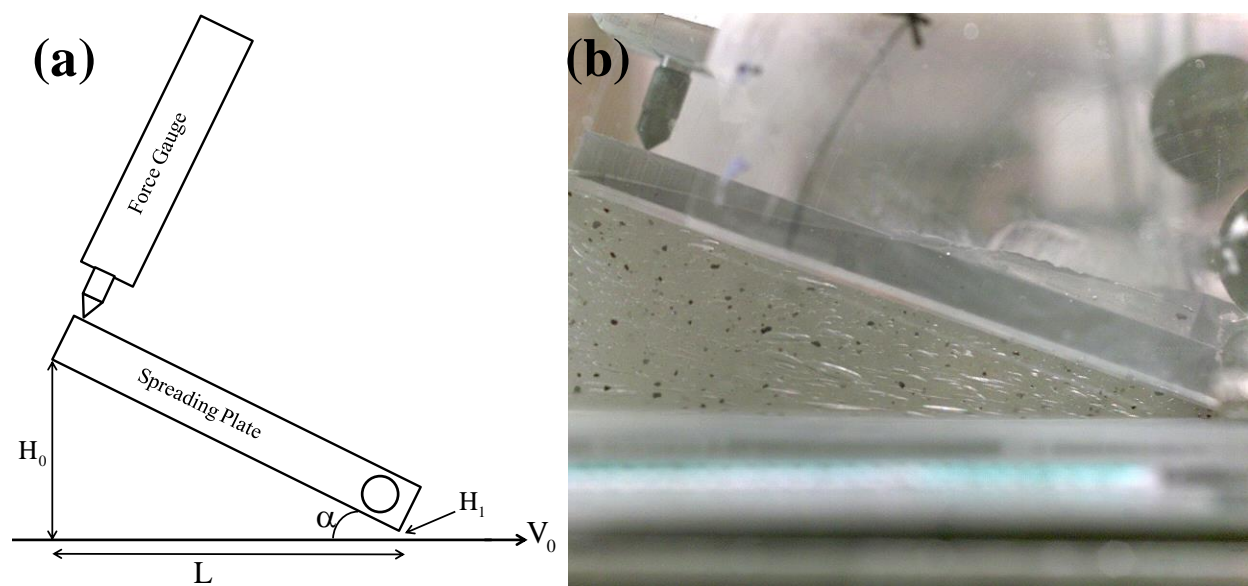


Fig. 3. Sketch (a) and image (b) of the experimental setup with the 20° angle of inclination of the spreading plate. In the image black seeding particles are seen inside Carbopol.

The wedge-like gap of the spreading setup shown in Fig. 3 was adjusted by varying the exit height and the angle of inclination of the spreading plate, which pivots freely about the exit point. A wet film thickness gauge was used to measure the thickness of the layer gel after it exited from the wedge-like gap. It appeared to be equal to the exit height H_1 since practically no swelling was found (which means that the gel was inelastic). It should be emphasized that in the present experiments (and in our previous works with Carbopol 940) the viscous forces are much greater than the elastic forces (if any) at the shear rates relevant to the wedge geometry. In this study the exit height H_1 ranged between 0.6 mm and 1.5 mm at the three inclination angles, 5° , 10° , and 20° . The velocity of the moving surface was either 0.167 m/s or 0.240 m/s. The range of the parameters chosen is characteristic of the applications. The length of the material ribbon applied onto the moving surface varied between 1 m and 1.25 m creating a steady-state flow in the wedge-like gap for approximately 5 to 6 s.

Image analysis

Images were captured using a Phantom Miro eX4 high speed camera at a rate of 100 fps with a screen size of 800 pixels by 600 pixels capturing an image approximately 15 cm by 11 cm giving each pixel a size of 0.019 cm^2 . The frame speed produced a minimum of 50 images for processing one particle when the moving surface was traveling at 0.24 m/s. Particles in the fluid approximately ranged from 3×3 pixels to 7×5 pixels or 0.57 mm by 0.57 mm to 1.33 mm by 0.95 mm, respectively. Identifying the particles position was done manually with assistance from a computer code. The user would identify a particle (using a zoomed image) and click on it, the program would then note its position and time. Next, the user would skip a number of frames

until the particle moved a significant amount, then the user would again click on the particle and the program would note its new position and time. Since the particles were tracked manually, no general error calculation can be made. As an example highlighting the maximum error, if a 7 pixel particle moved 1 cm between marked locations and time, the largest error would be 13%. However, zooming in on the image greatly decreased the possible error because the center pixel of each particle was easily visible. In some cases it was difficult to gather data in regions near the top plate and the exit; therefore, these regions were left blank.

Results

Velocity profiles

Since Carbopol gels reveal pseudoplastic power-law rheology in shear flow, it is expected that there should be practically no flow inside such domains where the shear rate is relatively low. Indeed, effective viscosity of the gels corresponding to these domains should be very high, or alternatively the shear stress there should be lower than the yield stress. Therefore, with Carbopol being the working fluid it might be found that inside the boundaries of these domains one would expect to see a stagnation zone, rather than a reverse flow for Newtonian fluids, which is, indeed, corroborated by the experimental data on the left as panels (a) in Figs. 4 – 11.

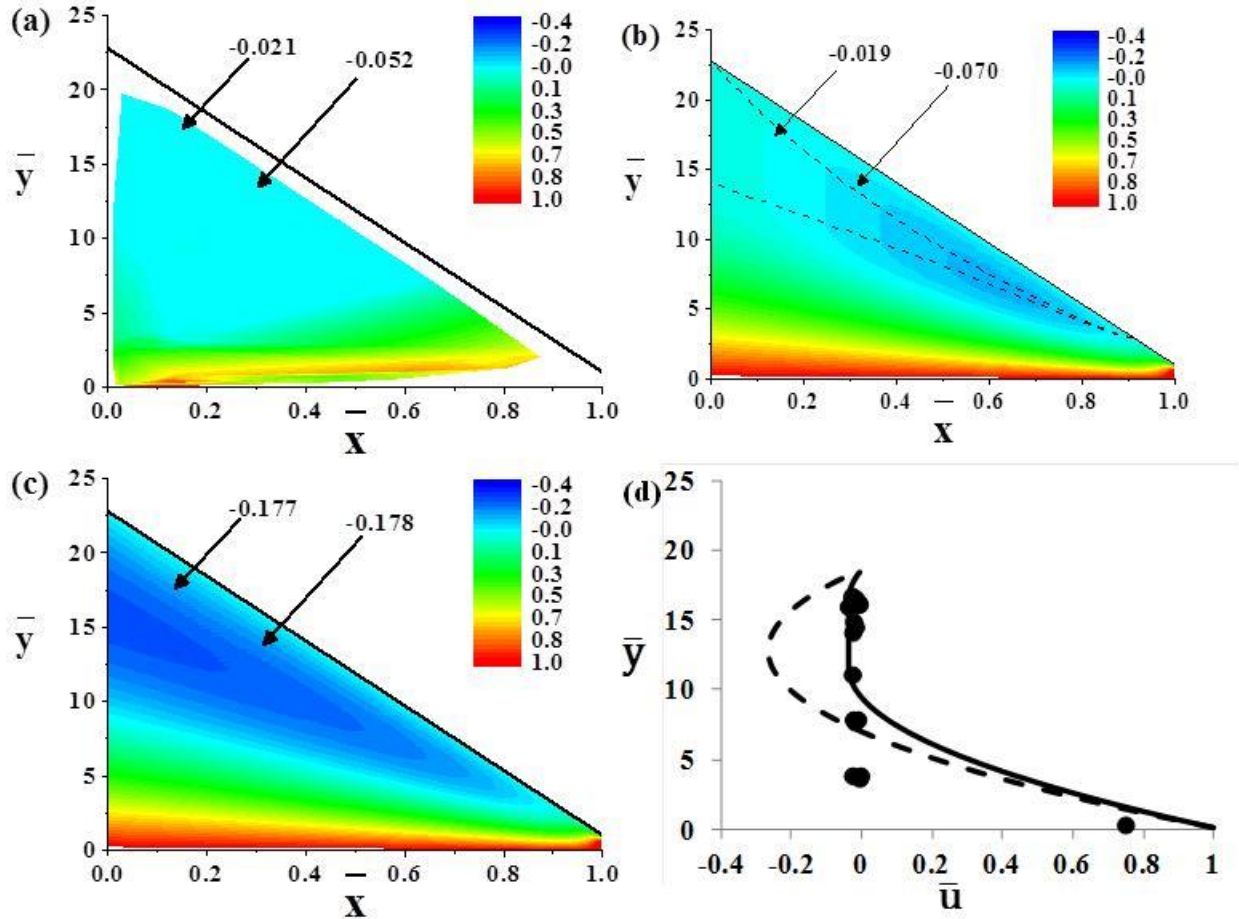


Fig. 4. Experimental velocity fields measured for Carbopol gel (a) under a wedge at $\alpha = 5^\circ$ and $H_1 = 0.6$ mm versus the corresponding theoretical velocity fields for: (b) Bingham fluid with a floating core from $\bar{x} = 0$ to $\bar{x} = 0.92$, and no core, or Newtonian profile, from $\bar{x} = 0.92$ to $\bar{x} = 1$; and (c) Newtonian fluid. Legend shows the dimensionless velocity values where the wall velocity used as a scale is 0.167 m/s. Arrows in panel (a) point to representative velocities in the respective region of flow and in panels (b) and (c) the theoretical velocities are given at the same respective location as in (a). The notation \bar{x} corresponds to the longitudinal coordinate x rendered dimensionless by L [cf. Figs. 1 and 3(a)]. Panel (d) shows the theoretical velocity profiles at $\bar{x} = 0.2$ (for the Bingham fluid-by solid line, and for the Newtonian one- by dashed

line), as well as the experimental data for the velocity profile at $\bar{x} = 0.2 \pm 0.015$ shown by symbols. The dashed lines in panel (b) outline the region of the floating core.

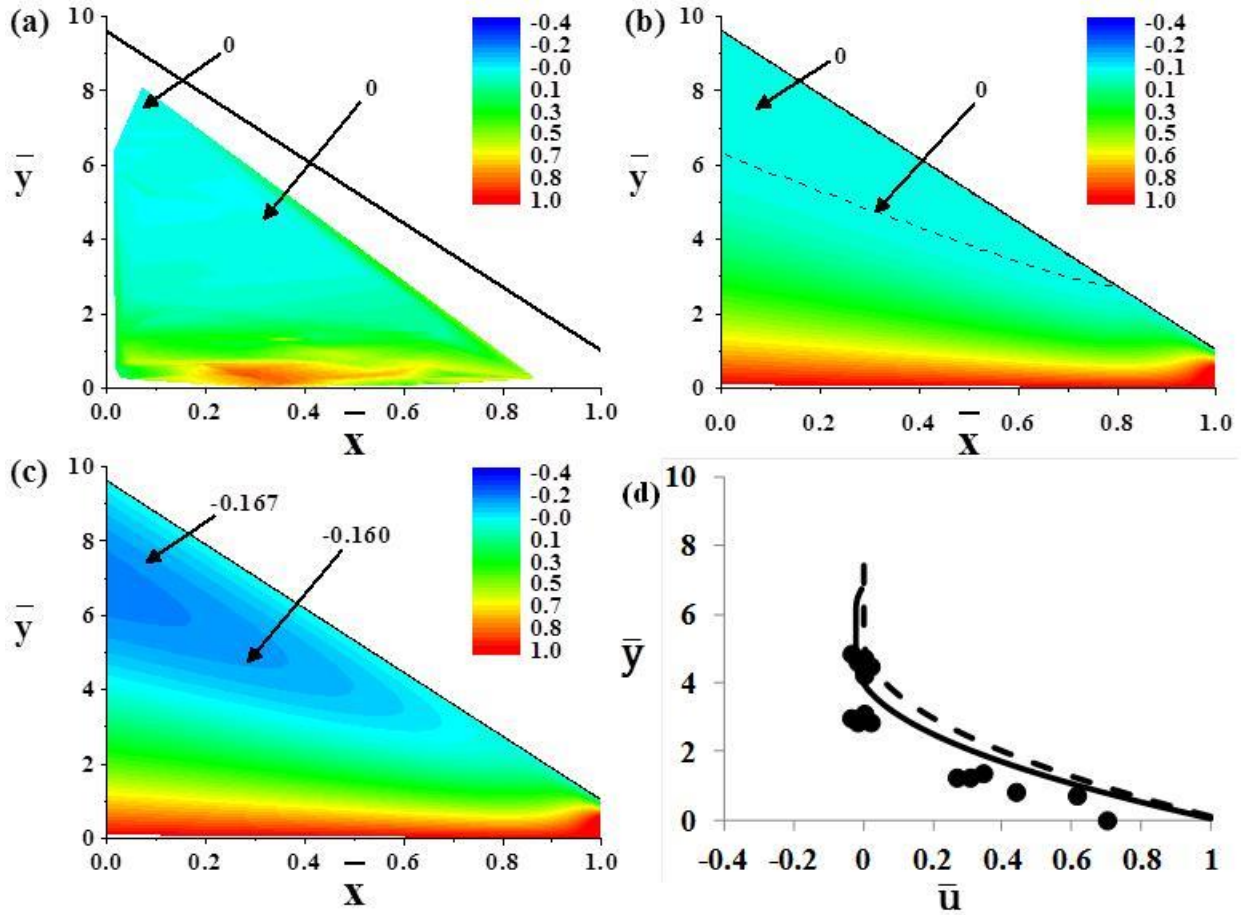


Fig. 5. Experimental velocity fields measured for Carbopol gel (a) under a wedge at $\alpha = 5^\circ$ and $H_1 = 1.5$ mm versus the corresponding theoretical velocity fields for a (b) Bingham fluid with an attached upper core from $\bar{x} = 0$ to $\bar{x} = 0.80$, and no core, or Newtonian profile, from $\bar{x} = 0.80$ to $\bar{x} = 1$; and (c) Newtonian fluid. Legend shows the dimensionless velocity values where the wall velocity used as a scale is 0.167 m/s. Arrows in panel (a) point to representative velocities in the respective region of flow and in panels (b) and (c) the theoretical velocities are given at the same

respective location as in (a). Panel (d) shows the theoretical velocity profiles at $\bar{x} = 0.33$ (for the Bingham fluid-by solid line, and for the Newtonian one- by dashed line), as well as the experimental data for the velocity profile at $\bar{x} = 0.33 \pm 0.02$ shown by symbols. The dashed lines in panel (b) outline the region of the floating core.

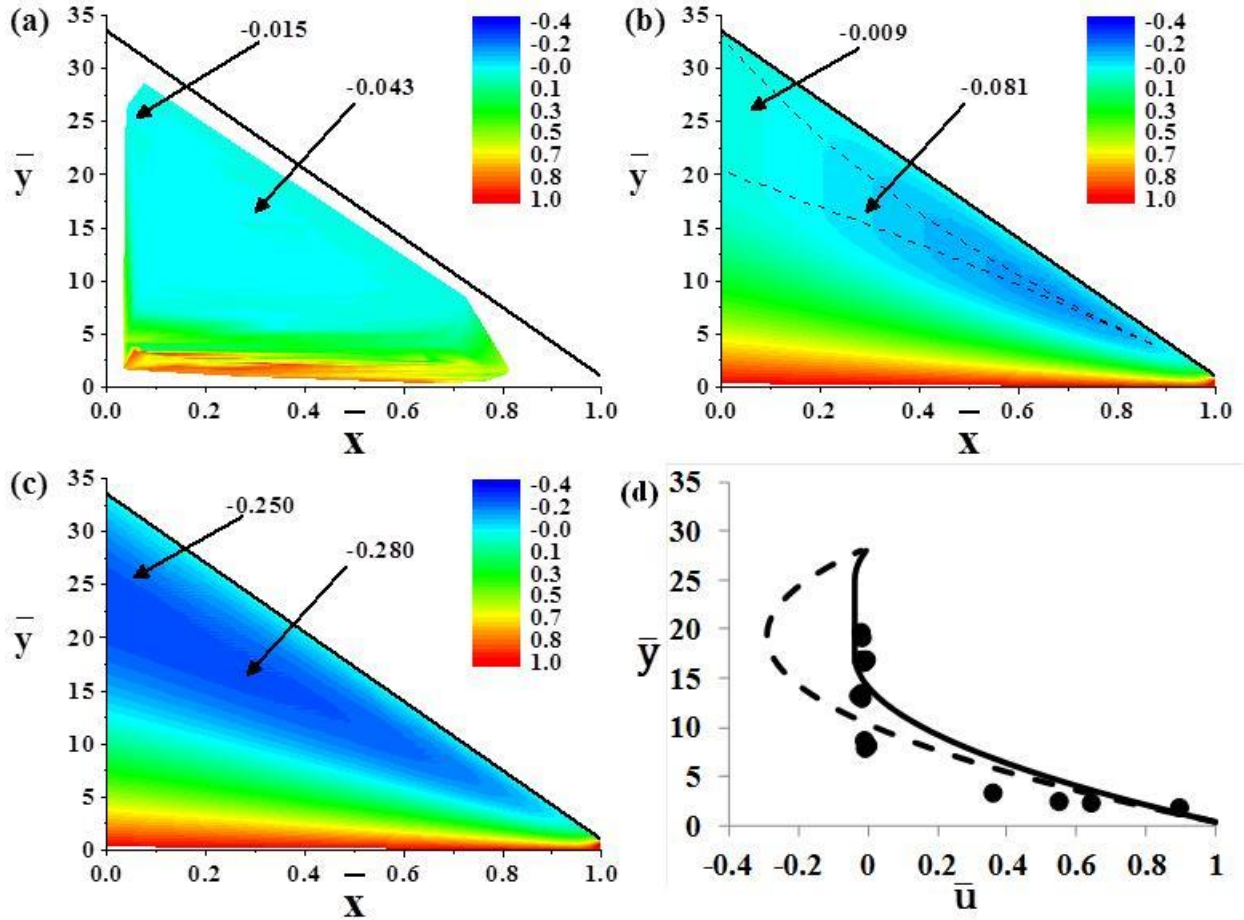


Fig. 6. Experimental velocity fields measured for Carbopol gel (a) under a wedge at $\alpha = 10^\circ$ and $H_1 = 0.8$ mm versus the corresponding theoretical velocity fields for a (b) Bingham fluid with a floating core from $\bar{x} = 0$ to $\bar{x} = 0.95$, and no core, or Newtonian profile, from $\bar{x} = 0.95$ to $\bar{x} = 1$; and (c) Newtonian fluid. Legend shows the dimensionless velocity values where the wall

velocity used as a scale is 0.167 m/s. Arrows in panel (a) point to representative velocities in the respective region of flow and in panels (b) and (c) the theoretical velocities are given at the same respective location as in (a). Panel (d) shows the theoretical velocity profiles at $\bar{x} = 0.17$ (for the Bingham fluid-by solid line, and for the Newtonian one- by dashed line), as well as the experimental data for the velocity profile at $\bar{x} = 0.175 \pm 0.015$ shown by symbols. The dashed lines in panel (b) outline the region of the floating core.

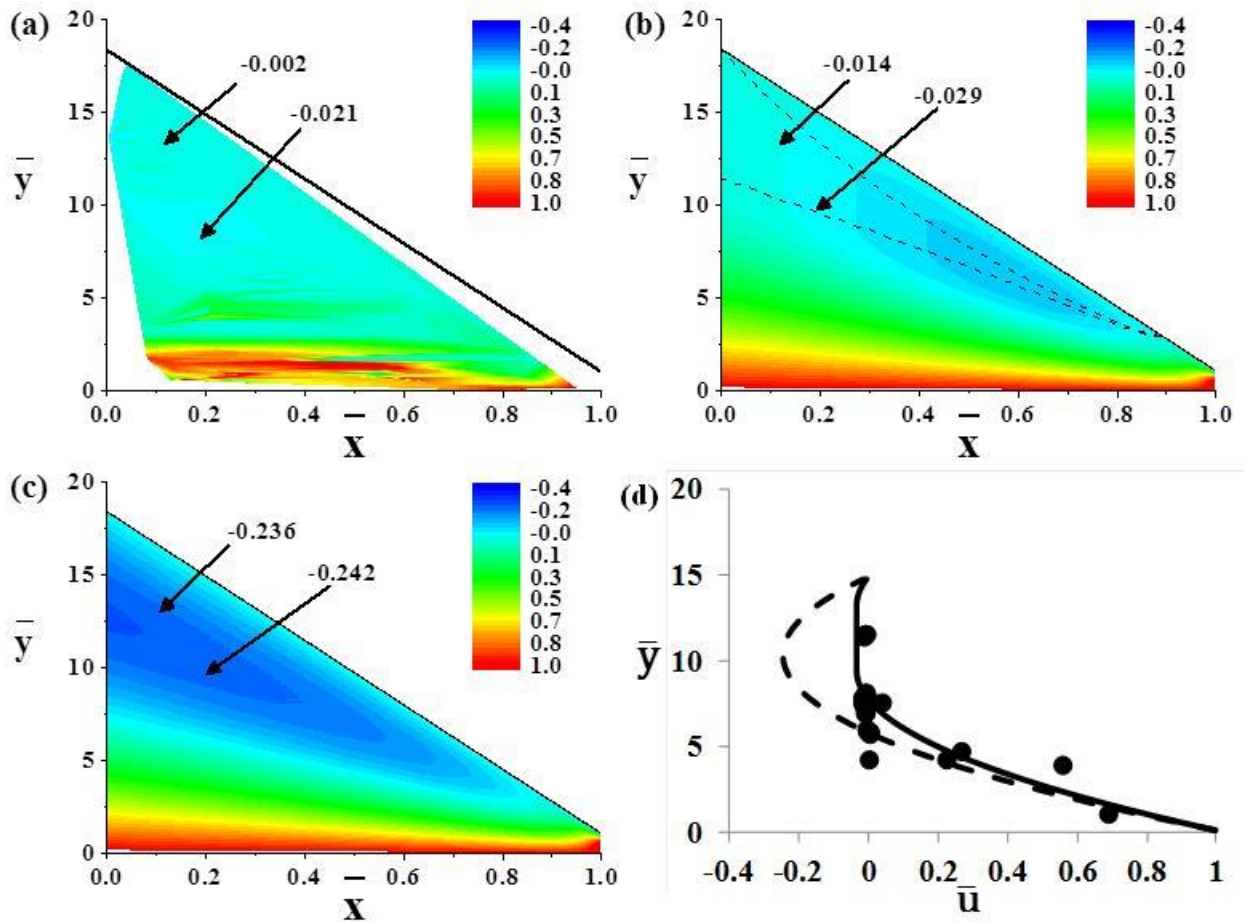


Fig. 7. Experimental velocity fields measured for Carbopol gel (a) under a wedge at $\alpha = 10^\circ$ and $H_1 = 1.5$ mm versus the corresponding theoretical velocity fields for a (b) Bingham fluid with a

floating core from $\bar{x} = 0$ to $\bar{x} = 0.90$, and no core, or Newtonian profile, from $\bar{x} = 0.90$ to $\bar{x} = 1$; and (c) Newtonian fluid. Legend shows the dimensionless velocity values where the wall velocity used as a scale is 0.167 m/s. Arrows in panel (a) point to representative velocities in the respective region of flow and in panels (b) and (c) the theoretical velocities are given at the same respective location as in (a). Panel (d) shows the theoretical velocity profiles at $\bar{x} = 0.21$ (for the Bingham fluid-by solid line, and for the Newtonian one- by dashed line), as well as the experimental data for the velocity profile at $\bar{x} = 0.21 \pm 0.01$ shown by symbols. The dashed lines in panel (b) outline the region of the floating core.

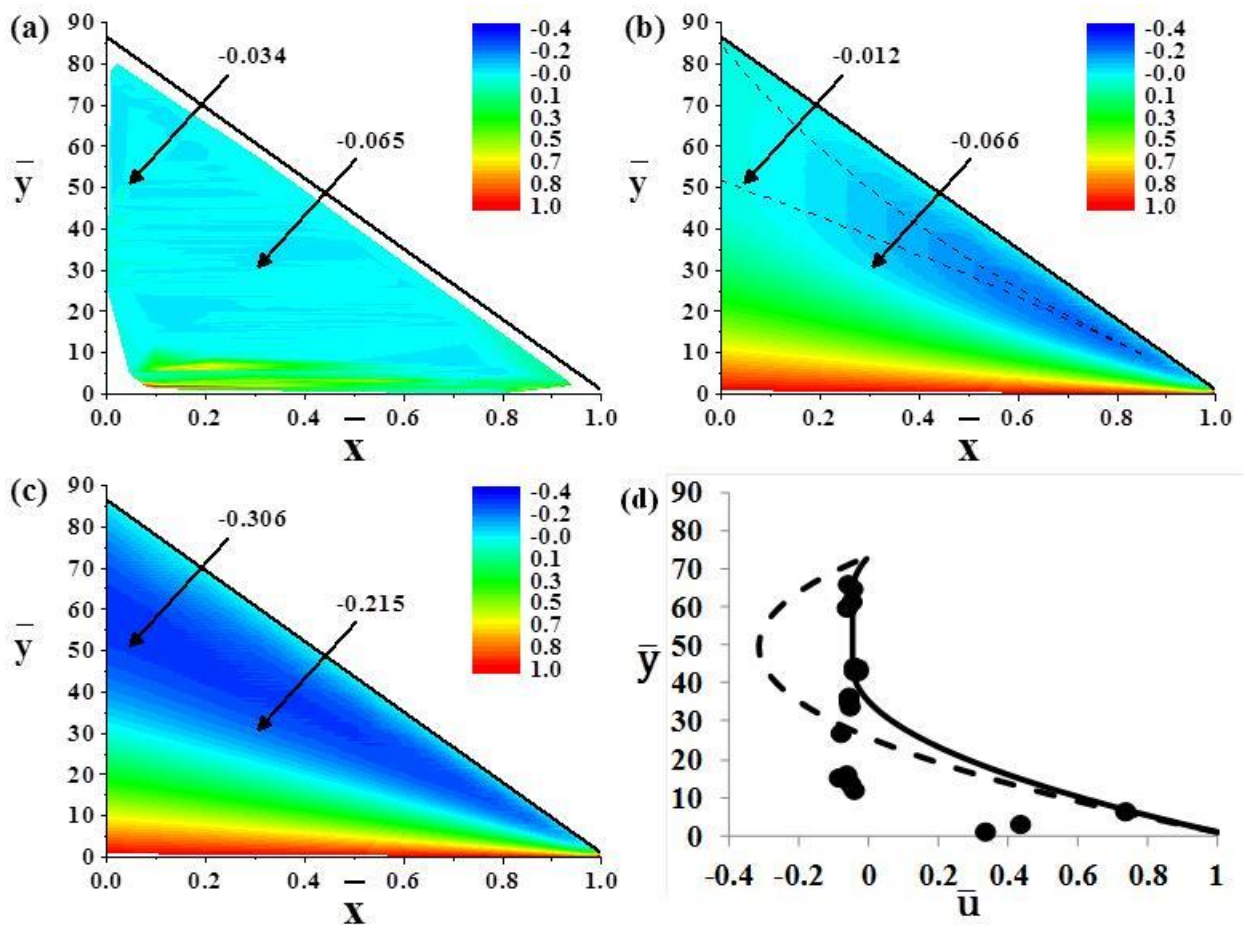


Fig. 8. Experimental velocity fields measured for Carbopol gel (a) under a wedge at $\alpha = 20^\circ$ and $H_1 = 0.6$ mm versus the corresponding theoretical velocity fields for a (b) Bingham fluid with a floating core from $\bar{x} = 0$ to $\bar{x} = 0.98$, and no core, or Newtonian profile, from $\bar{x} = 0.98$ to $\bar{x} = 1$; and (c) Newtonian fluid. Legend shows the dimensionless velocity values where the wall velocity used as a scale is 0.167 m/s. Arrows in panel (a) point to representative velocities in the respective region of flow and in panels (b) and (c) the theoretical velocities are given at the same respective location as in (a). Panel (d) shows the theoretical velocity profiles at $\bar{x} = 0.16$ (for the Bingham fluid-by solid line, and for the Newtonian one- by dashed line), as well as the experimental data for the velocity profile at $\bar{x} = 0.155 \pm 0.015$ shown by symbols. The dashed lines in panel (b) outline the region of the floating core.

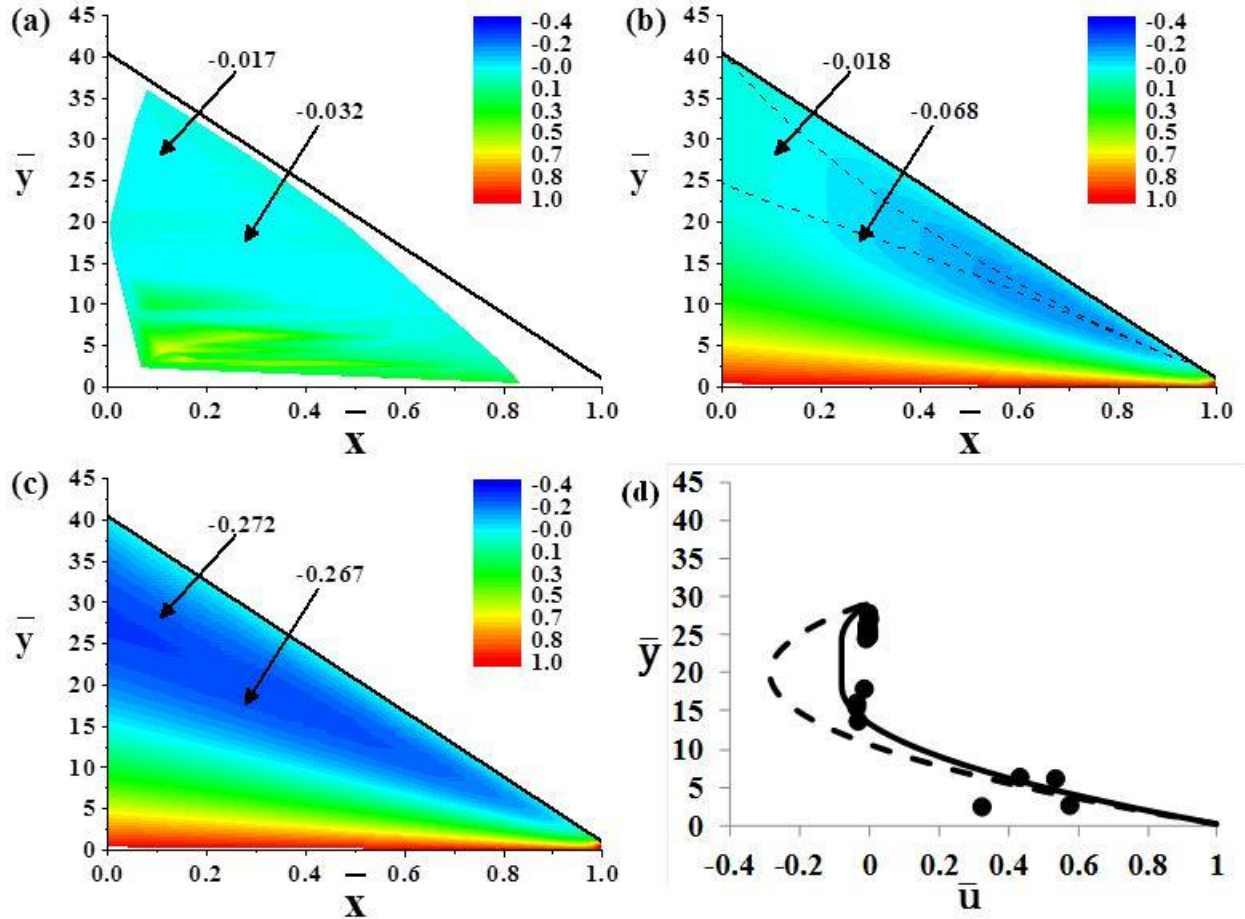


Fig. 9. Experimental velocity fields measured for Carbopol gel (a) under a wedge at $\alpha = 20^\circ$ and $H_1 = 1.3$ mm versus the corresponding theoretical velocity fields for a (b) Bingham fluid with a floating core from $\bar{x} = 0$ to $\bar{x} = 0.96$, and no core, or Newtonian profile, from $\bar{x} = 0.96$ to $\bar{x} = 1$; and (c) Newtonian fluid. Legend shows the dimensionless velocity values where the wall velocity used as a scale is 0.167 m/s. Arrows in panel (a) point to representative velocities in the respective region of flow and in panels (b) and (c) the theoretical velocities are given at the same respective location as in (a). Panel (d) shows the theoretical velocity profiles at $\bar{x} = 0.29$ (for the Bingham fluid-by solid line, and for the Newtonian one- by dashed line), as well as the

experimental data for the velocity profile at $\bar{x} = 0.295 \pm 0.015$ shown by symbols. The dashed lines in panel (b) outline the region of the floating core.

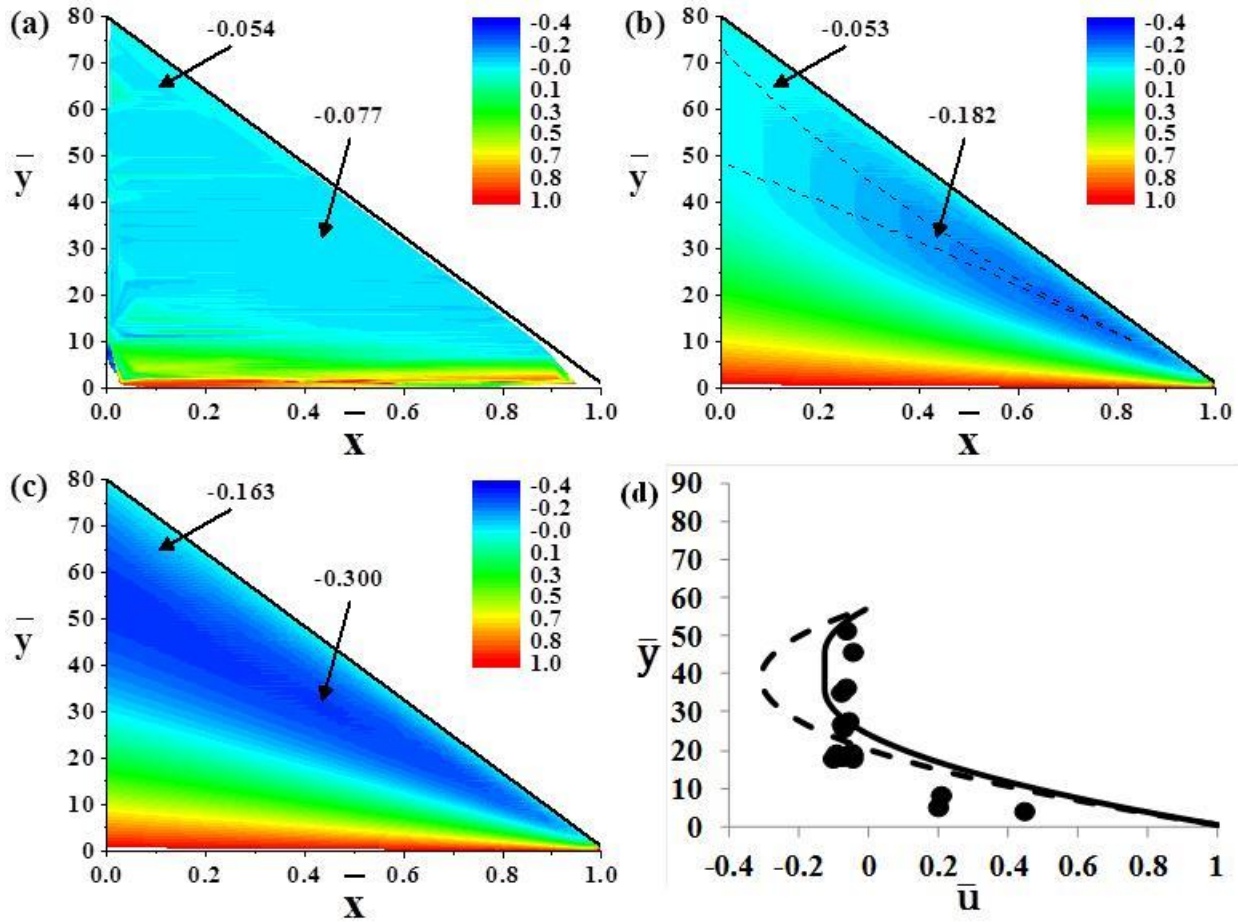


Fig. 10. Experimental velocity fields measured for Carbopol gel (a) under a wedge at $\alpha = 20^\circ$ and $H_1 = 0.65$ mm versus the corresponding theoretical velocity fields for a (b) Bingham fluid with a floating core from $\bar{x} = 0$ to $\bar{x} = 0.98$, and no core, or Newtonian profile, from $\bar{x} = 0.98$ to $\bar{x} = 1$; and (c) Newtonian fluid. Legend shows the dimensionless velocity values where the wall velocity used as a scale is 0.240 m/s. Arrows in panel (a) point to representative velocities in the

respective region of flow and in panels (b) and (c) the theoretical velocities are given at the same respective location as in (a). Panel (d) shows the theoretical velocity profiles at $\bar{x} = 0.29$ (for the Bingham fluid-by solid line, and for the Newtonian one- by dashed line), as well as the experimental data for the velocity profile at $\bar{x} = 0.295 \pm 0.015$ shown by symbols. The dashed lines in panel (b) outline the region of the floating core.

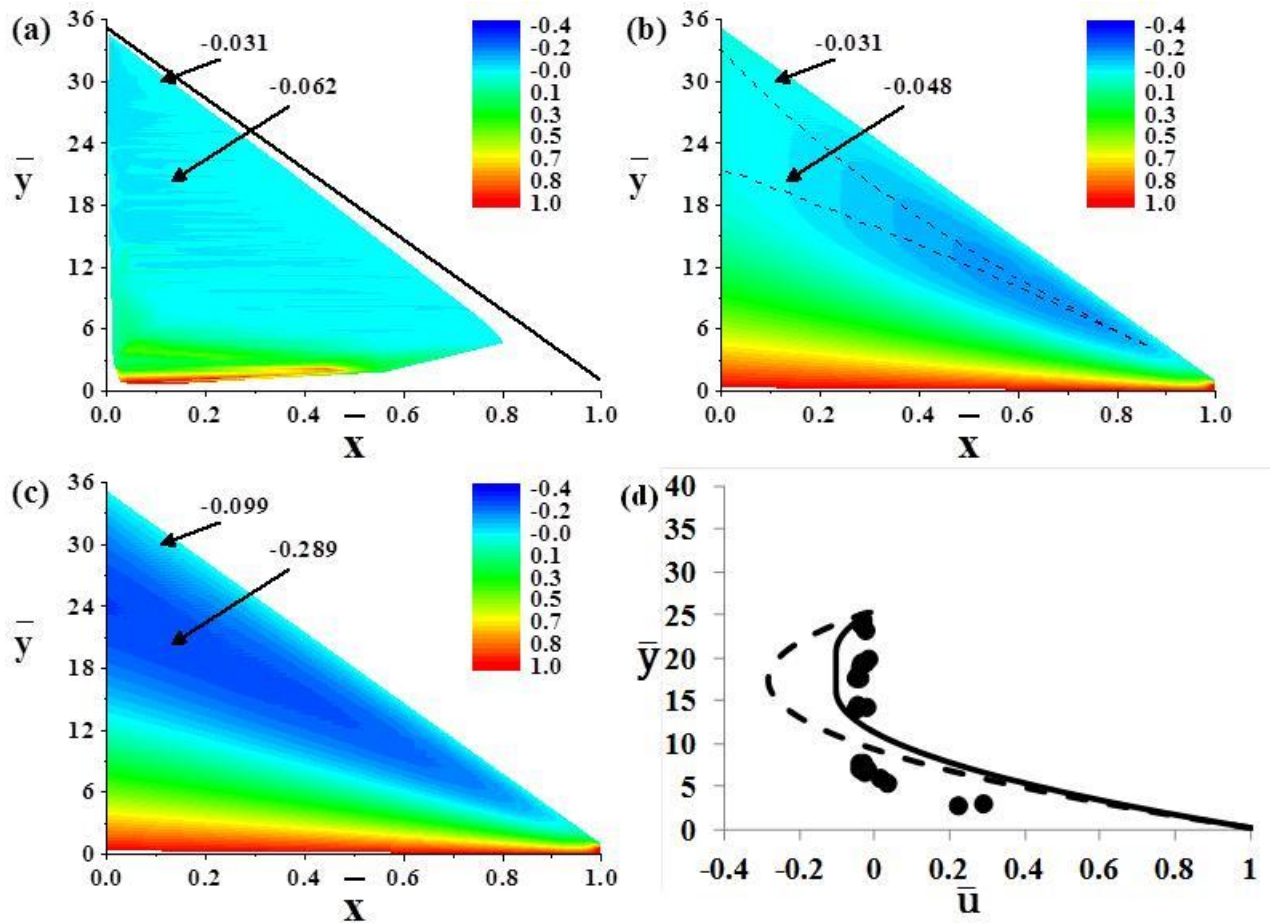


Fig. 11. Experimental velocity fields measured for Carbopol gel (a) under a wedge at $\alpha = 20^\circ$ and $H_1 = 1.5$ mm versus the corresponding theoretical velocity fields for a (b) Bingham fluid with a floating core from $\bar{x} = 0$ to $\bar{x} = 0.95$, and no core, or Newtonian profile, from $\bar{x} = 0.95$ to

$\bar{x} = 1$; and (c) Newtonian fluid. Legend shows the dimensionless velocity values where the wall velocity used as a scale is 0.240 m/s. Arrows in panel (a) point to representative velocities in the respective region of flow and in panels (b) and (c) the theoretical velocities are given at the same respective location as in (a). Panel (d) shows the theoretical velocity profiles at $\bar{x} = 0.29$ (for the Bingham fluid-by solid line, and for the Newtonian one- by dashed line), as well as the experimental data for the velocity profile at $\bar{x} = 0.295 \pm 0.015$ shown by symbols. The dashed lines in panel (b) outline the region of the floating core.

Experimentally found velocity profiles were observed for a number of the inclination angles (for some of them the lubrication approximation does not necessarily hold). The experimentally found velocities are contrasted to the theoretically predicted velocity profiles of a Bingham fluid and a Newtonian fluid at the inclination angle and exit height of 5° and 0.6 mm, respectively, in Fig. 4, 5° and 1.5 mm in Fig. 5, 10° and 0.8 mm in Fig. 6, 10° and 1.5 mm in Fig. 7, 20° and 0.6 mm in Fig. 8, 20° and 1.3 mm in Fig. 9, and at a higher velocity of the moving surface at 20° and 0.65 mm in Fig. 10, as well as 20° and 1.5 mm in Fig. 11. The experimental velocity is rendered dimensionless by the speed of the conveyer belt pulling the fluid. In each of the experimental plots, arrows pointing to two positions in the reverse flow region identify a representative velocity in the respective area. Furthermore, the same positions are identified in the theoretical Bingham and Newtonian fluid velocity fields, which are labeled with the respective theoretical velocity in panels (b) and (c) in Figs. 4-11.

The theoretically predicted shear rate fields (Schlichting 1987) for Newtonian fluid are shown in Fig. 12. The domains with the low shear rate would be prone to stagnation in the case

of Carbopol due to either high effective viscosity or the shear stress lower than the yield stress, as is seen in Figs. 4 – 11 on the left [in panels (a)].

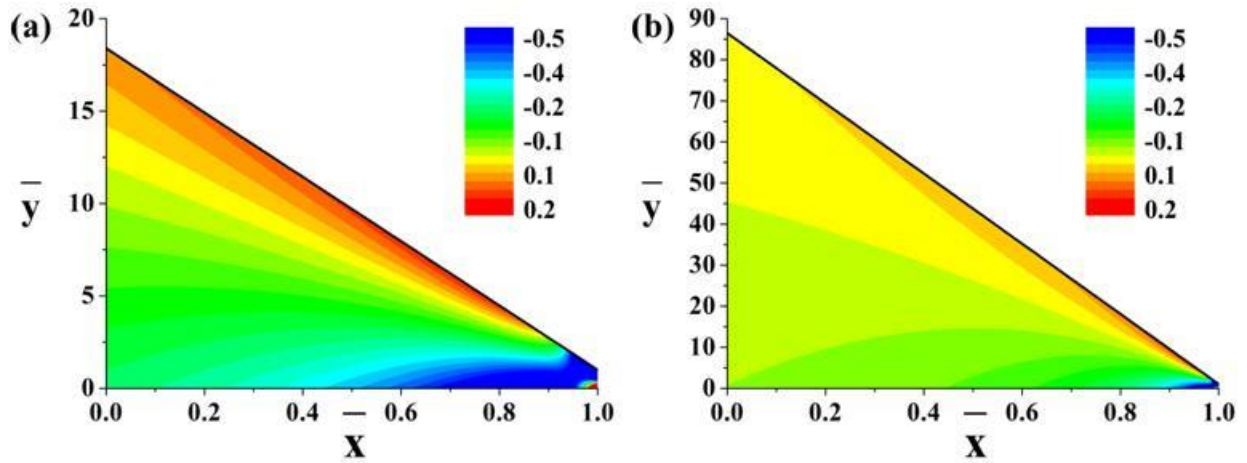


Fig. 12. Shear rate fields $d\bar{u}/d\bar{y}$ for Newtonian fluid for: (a) $\bar{H}_0 = 18.4$, and (b) $\bar{H}_0 = 86.5$. The notation \bar{u} is used for the longitudinal velocity rendered dimensionless by the wall velocity, and \bar{y} for the transversal coordinate rendered dimensionless by H_1 .

Fig. 13 reveals the presence of the reverse flow near the inclined plate, with particle 1 moving backward, while particle 2 moving forward.

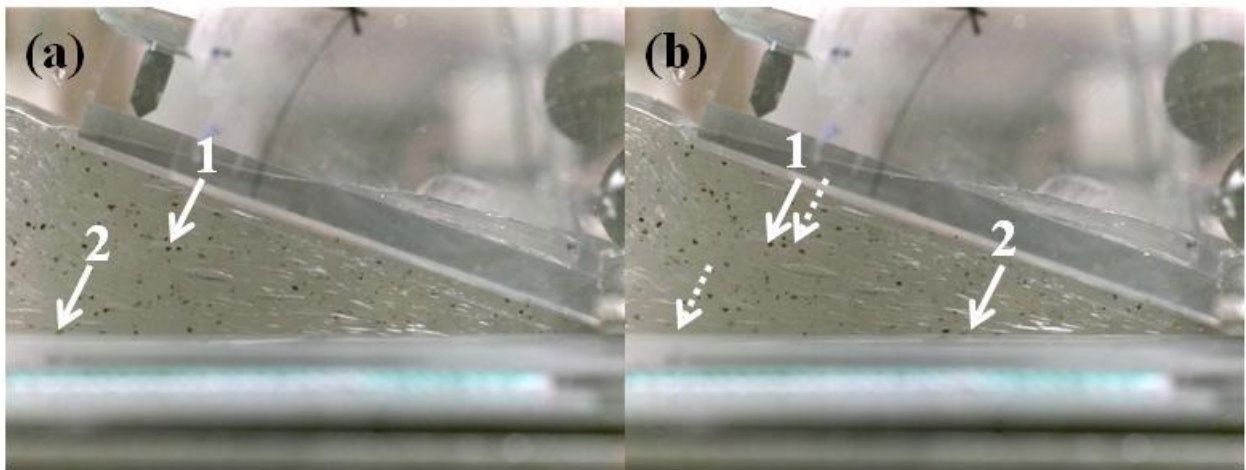


Fig. 13. Two consecutive images of seeding particles 0.5 s apart. The inclination angle is 20° , the exit height is 0.65 mm, and the velocity of the moving surface is 0.24 m/s. Solid arrows in panel (a) point to two specific particles, and dashed arrows in panel (b) point to the same particles in 0.5 s.

Figs. 14 and 15 illustrate the presence of an attached upper core and a floating core in the flow. In the two consecutive images in Fig. 14 particles 1 and 2 are at rest relative to the motionless spreading plate. On the other hand, in Fig. 15 at a higher inclination angle it is seen that all three highlighted particles move in the reverse flow region, with particles 2 and 3 being faster than particle 1.

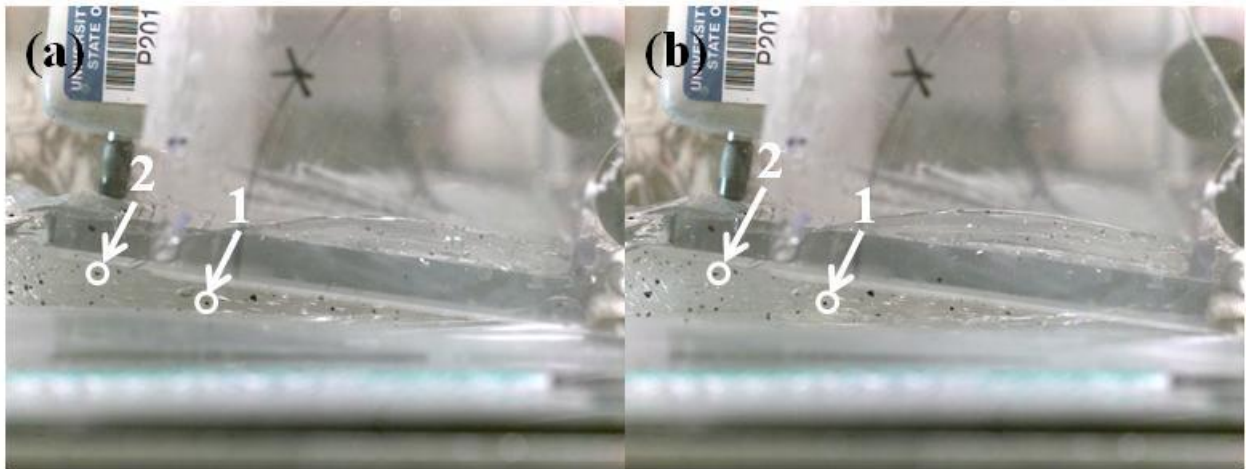


Fig. 14. Stagnation zone close to the inclined spreading plate. The inclination angle of the plate is 5° with the exit height of 1.5 mm; $\overline{H}_0 = 6$ [rendered dimensionless by H_1 -cf. Fig. 3(a)]. The two consecutive images are taken 3 s apart. Arrows point to two seeding particles (encircled) that reveal no motion.

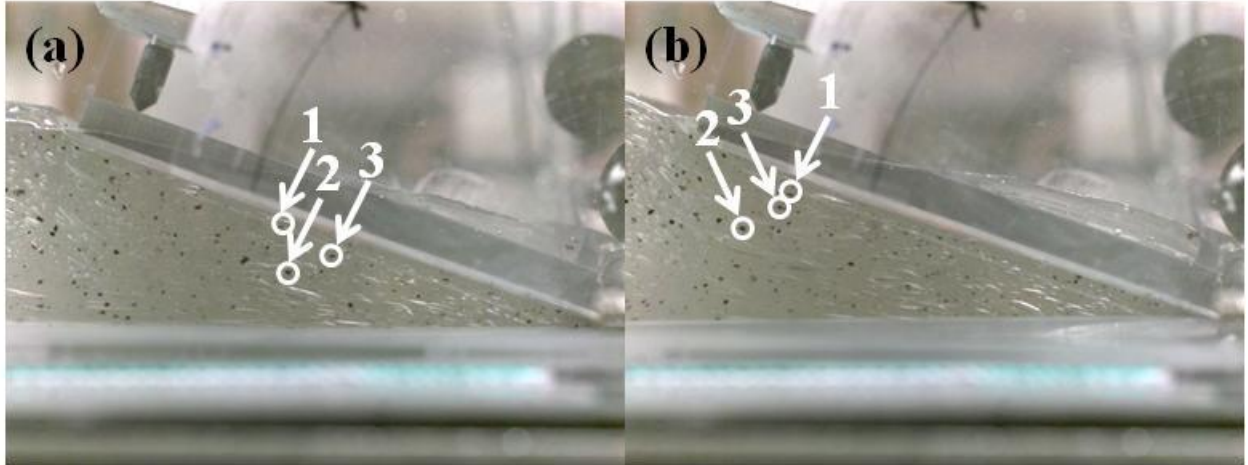


Fig. 15. Plug flow within the reverse flow region. The angle of the spreading plate inclination is 20° with the exit height of 0.650 mm ; $\overline{H}_0 = 79.9$. The two consecutive images are taken 4 s apart. All three particles (encircled) move in the reverse direction, with particle 1 being slower than particles 2 and 3.

Rheological properties

If one assumes a Newtonian-like behavior, the restraining force $|\mathbf{F}_{\text{exp}}|$ applied to the inclined plate to keep it in the position measured in the experiment can be used to evaluate the effective viscosity of the gel pulled by the moving wall through the wedge-like gap using the available Newtonian solution in Schlichting (1987). The corresponding values are listed in Table 1.

For a Bingham fluid model, the theoretical velocity profiles in the case of a floating core (Tichy 1991) are sensitive to the dimensionless yield stress, $\overline{\tau}_0 = \tau_0 H / \mu V_0$. The dimensional yield stress, τ_0 , is a fixed parameter, the wedge geometry, H , and conveyer belt velocity, V_0 , are

known in each experiment. Therefore, the viscosity, μ , was adjusted accordingly so that the theoretical velocity at the points indicated by the arrows in Figs. 4-11 closely matched the velocities found experimentally. The corresponding values are presented in Table 1.

Table 1. Experimental parameters and the calculated viscosity found using the Newtonian model in Schlichting (1987), and the Bingham model in Tichy (1991). The shear rate at the cross-section where the pressure gradient is zero, $\dot{\gamma}|_{dp/dx=0}$, is calculated from the pressure distribution using the Newtonian model.

Angle (deg)	Exit height, H_1 (mm)	\overline{H}_0	Velocity (m/s)	Force (N)	Newtonian viscosity (Pa \times s)	$\dot{\gamma} _{dp/dx=0}$ (1/s)	Yield stress (Pa)	Bingham viscosity (Pa \times s)
5	0.6	22.8	0.167	19.1	4.8	101	570	43
5	1.5	9.6	0.167	15.0	6.0	41	570	$\leq 50^{**}$
10	0.8	33.6	0.167	13.5	11.8	79	570	83
10	1.5	18.4	0.167	7.9	8.6	41	570	89
20	0.6	86.5	0.167	8.1	22.5	103	570	155
20	1.3	40.5	0.167	6.8	21.8	50	570	155
20	0.65	79.9	0.240	9.8	19.2	143	570	130
20	1.5	35.2	0.240	9.7	22.5	59	570	130

** The dimensionless theoretical Bingham velocity profile for an attached upper core is independent of the yield stress; therefore the viscosity value was obtained by identifying the yield stress which set such a core.

Discussion

When a yield-stress fluid is pulled into a wedge, there are three regions of flow that are of interest. The first region exists near the moving wall (the conveyor belt) where the shear stress is high and fluid is pulled forward albeit an adverse pressure gradient. The second region is near

the exit where the pressure gradient is no longer positive (no longer adverse) causing fluid motion forward in addition to the pull provided by the moving wall. The third region is far from moving conveyer belt (toward the inclined wall) where the adverse pressure gradient is dominant causing reverse flow to occur. In other words, fluid moves against the direction of the conveyer belt motion in the third region.

Comparison of velocity profiles

Near the moving wall, the shear rate is high and the Bingham fluid and Newtonian fluid models result in approximately the same theoretical velocity profiles. It should be emphasized that the forward flow regions, designated by colors from green to red in Figs. 4 – 11, found from the experiments are in good agreement, in magnitude and position, with both the Bingham and Newtonian theoretical results also depicted in these figures. The agreement is better when \overline{H}_0 is small. As \overline{H}_0 increases the experimentally found forward velocity region is smaller in height compared to the predicted value in either model, although it still shows similar magnitudes. This discrepancy is likely due to comparing a shear-thinning fluid in experiment to theoretical Bingham and Newtonian models.

At the location, on the horizontal axis, where the pressure gradient becomes zero, the flow is in a state of pure shear. In the Bingham model, it means that at this location the flow of a yield-stress fluid is similar to that of a Newtonian fluid; i.e. it has no plug zone, as the shear rate is high in this zone. This location is stated in the caption of each Fig. 4-11. After this location, the negative pressure gradient and the moving bottom wall both propel the fluid towards the exit.

Note that in this region a plug can occur but since this region represents such a minute part of our experiment, and it is difficult to resolve in the images, the plug (if any) could not be resolved and the flow is modeled using the Newtonian velocity profile. In Figs. 7, 8, and 10 the velocity near the exit is found experimentally and agrees with both theoretical models.

Far from the moving bottom wall, the shear stress decreases and the adverse pressure gradient is able to push the fluid backwards creating a region of reverse flow. It is in this region where the greatest distinction between a Newtonian and Bingham fluid models occurs.

As in any pressure-driven flow, if the same pressure gradient is applied to push a Newtonian fluid and a Bingham fluid of comparable viscosity, it is expected that the Newtonian fluid will have a higher velocity. This is the case for the reverse flow region of the wedge. In the theoretical Newtonian model the velocity profile shows strong reverse flow which intensifies as \overline{H}_0 increases. In the experiments, the reverse velocity does increase with increasing \overline{H}_0 but not nearly as dramatically as the Newtonian model predicts. At the lowest entrance height used shown in Fig. 5, $\overline{H}_0 = 9.6$, the experimental velocity profile shows that fluid above $\overline{y} \approx 4$ has zero velocity (confirmed by the images in Fig. 14). However, the Newtonian model predicts the velocity values at the coordinates designated by the arrows in the image as $\overline{u} = -0.167$ and $\overline{u} = -0.160$. In the experiments where there exists a reverse flow velocity, Figs. 4 and 6-11, the Newtonian model overpredicts the magnitude of the velocity, sometimes by an order of magnitude. Comparing the experimental velocity fields to the theoretical Newtonian ones emphasizes the role that the yield stress plays in the development of the reverse flow profile.

Despite the discrepancy in the theoretical velocity flow field predicted by the Newtonian fluid model compared to the experimental data, relevant information from the measured force

can be obtained using this model. This is especially important since the pressure profile cannot be explicitly obtained in the case of a Bingham fluid.

The measured force gauge data in Table 1 reveals three trends found in the experiments with Carbopol gels that agree with the predictions of the Newtonian fluid model for the restraining force. The first trend is observed when keeping the exit height, H_1 , constant; then, the force decreases as \overline{H}_0 increases. The second trend is that the force decreases when keeping \overline{H}_0 constant, but increasing H_1 . The third trend was observed when the velocity of the moving surface increased, where both H_1 and \overline{H}_0 being kept constant: the force increased.

The theoretical velocity field predicted using the Bingham fluid model illustrates how the yield stress of the fluid can arrest or slow down the flow in the reverse flow region. An example of the fluid motion in the reverse flow region being arrested can be seen in Fig. 5 where $\overline{H}_0 = 9.6$. This agrees with the velocity profile for a Bingham fluid shown in Fig. 5(b) which has an attached upper core. The viscosity value, shown in Table 1, for this case was determined by identifying the lowest viscosity value at which the criteria for a floating core case (cf. Tichy 1991) is not met at the entrance of the wedge. In other words, a viscosity value less than or equal to $50 \text{ Pa}\cdot\text{s}$ satisfies the condition for an attached upper core and a viscosity value greater than $50 \text{ Pa}\cdot\text{s}$ would make the criteria for a floating core to be true.

At higher angles of inclination of the spreading plate, the adverse pressure gradient is sufficient to generate reverse flow illustrated by the motion of particles 2 and 3 in Fig. 15 relative to the spreading plate which is at rest. The respective position of these two particles does not change, which reveals that there is a plug flow core in the reverse flow zone. Examples of fluid being slowed due to the yield stress in the reverse flow region are shown in Figs. 4, and 6 – 11.

The images highlighting a floating core in Fig. 15 correspond to the experimental data in Fig. 10. The experimental velocity profiles [Figs. 4(a), 6(a) – 11(a)] show that the reverse flow velocity at the points indicated by the arrows ranges from $\bar{u} = -0.015$ to $\bar{u} = -0.077$, albeit when $\bar{H}_0 = 18.4$ there is $\bar{u} = -0.002$. The theoretical velocities for the Bingham fluid model [Figs. 4(b), 6(b) – 11(b)] at the indicated points show velocity values ranging from $\bar{u} = -0.009$ to $\bar{u} = -0.081$, albeit when $\bar{H}_0 = 79.9$ the theoretical reverse velocity at one point is $\bar{u} = -0.182$. In general, the magnitude and location of the theoretical velocity values found for the Bingham fluid model are in very good agreement with the experimental velocity values.

The values of the dimensionless velocities revealed in Figs. 13-15 are listed in Table 2.

Table 2. Velocity of highlighted particles in Figs. 13-15.

Figure number	Particle number	Dimensionless velocity, \bar{u}
13	1	-0.041
13	2	0.653
14	1	0
14	2	0
15	1	-0.032
15	2	-0.048
15	3	-0.051

However, there is one consistent discrepancy between the experimental velocity data and the predictions of the Bingham rheological model. That is, the predicted maximum reverse flow nearer to the exit, designated by the dark blue color in Figs. 4-11, was never obtained in the experiment.

Unlike the Newtonian model, the pressure distribution for the Bingham fluid model is not fully realizable. Therefore, calculating the viscosity from the Bingham model, as was done for the Newtonian fluid, is impossible.

The comparison of the predictions of the Newtonian and the Bingham models to the experimental data has elucidated the advantages and disadvantages of both models. Near the moving wall, where the shear stress is high and no core is formed, both types of the velocity profiles predicted by these models agree with the experimental data. Also, near the wedge exit both models agree with the experiment because the shear stresses cause the fluid to act Newtonian like and theoretically the Bingham model reduces to the Newtonian model since the conditions necessary to create a core are not fulfilled (i.e. the shear stresses are high). Only in the reverse flow region does the difference between the two models become evident. Experimentally, two rigid core types were identified, namely the attached upper core and the floating core. These cores had a dramatic influence on the reverse flow domain and were correctly predicted by the Bingham model. Although the theoretical Newtonian model was unable to reveal core formation, its closed form of the Reynolds equation (cf. Schlichting 1987) makes finding the pressure profile simple. With the pressure profile available, trends in the force acting on the wedge from the fluid under different wedge opening angles and the moving wall velocity were correctly predicted in the framework of the Newtonian model.

Comparison of viscosity values

The viscosity values listed in Table 1 present the results for the Newtonian fluid model found by from the measured restraining force. From Table 1, the evaluated Newtonian viscosities

were in the $4.8 \text{ Pa}\times\text{s}$ to $22.5 \text{ Pa}\times\text{s}$ range. The data obtained using parallel plate geometry with smooth plates, shown in Fig. 2, revealed Carbopol rheological parameters as $n = 0.16$ and $K = 154 \text{ Pa}\times\text{s}^n$. Using these parameters, the viscosity range found using the Newtonian model corresponds to the 88 s^{-1} and 13.6 s^{-1} shear rate range. At the location where the pressure gradient is zero, the shear rate, $\dot{\gamma}|_{dp/dx=0}$, is calculated and shown in Table 1. The calculated shear rates at the location where $dp/dx = 0$ are in agreement with the shear rates found using the parallel plate geometry. Furthermore, the shear rate near the moving plate can be calculated employing a rough estimate based on the predictions of both Newtonian and Bingham models that the shear rate below $\bar{y} = 0.2$ is roughly the same. Taking $\partial\bar{u}/\partial\bar{y} = (1-0.5)/(0.2-0) = 2.5$, the wall velocity $V_0 = 0.167 \text{ m/s}$, and evaluating $H_1 \approx 0.01 \text{ m}$, the dimensional shear rate is $\partial u/\partial y = 42 \text{ s}^{-1}$, and it increases nearer to the moving wall. It is then clear that near the exit and near the moving wall, the stress acting on the fluid must be greater than the yield stress, and thus the fluid flows as a Newtonian-like fluid.

Alternatively, the viscosity values for the Bingham fluid model were found by adjusting the viscosity (and thereby adjusting the dimensionless yield stress), so that the predicted velocity profile matched the experimental data. The viscosity values found using the Bingham model range from $43 \text{ Pa}\times\text{s}$ to $155 \text{ Pa}\times\text{s}$. Again using the rheological parameters found from the parallel plate geometry (Fig. 2), the viscosity values found for the Bingham model correspond to shear rates of 6.2 s^{-1} and 1.3 s^{-1} , respectively. The only region where this range of shear rates exists is in the reverse flow region near the core. Since the region near the plate has a similar shear rate to that of the Newtonian model and in the region near the exit the Bingham model coincides with the Newtonian model, adjusting the viscosity value had little effect in these high shear regions.

Therefore, the focus in fitting the Bingham model to match the experimental data was on the reverse flow region.

The regions near the exit and the moving wall represent the areas with the highest shear rates within the wedge where, accordingly, the fluid behaves as a Newtonian one. As one moves towards the reverse flow region, the shear rate decreases. When a varying shear rate exists, the power-law behavior of the fluid heavily influences the velocity profile (Tadmor and Gogos 2006). It is well known that Carbopol is a shear-thinning fluid (Curran et al. 2002; Coussot et al. 2009). Therefore, as the fluid is subject to lower shear rates farther from the moving surface where the adverse pressure gradient dominates, the viscosity of the fluid will increase and influence the flow behavior.

In the velocity profile corresponding to the Bingham fluid, the viscosity of the fluid had a direct impact on the configuration of the yield surface in the reverse flow, since the yield stress is a fixed parameter. In this reverse flow region, if a shear-rate dependence exists, it is relatively small compared to that near the moving wall and near the exit where the flow is practically Newtonian. Then, it is expected that the viscosity values for a pseudoplastic power-law fluid in a region of low shear reveal higher values of viscosity. Therefore, the viscosities found using the Bingham model are likely to represent the viscosity of Carbopol solution in the region of low shear. Furthermore, it seems that the combination of the two models (the Newtonian and Bingham ones) allows for a comprehensive understanding of how the viscosity of a power-law fluid changes due to the changing shear rate within the wedge flow.

Conclusion

The experimental and analytical velocity profiles for a Newtonian fluid are similar near the moving plate and near the exit where the shear stress overcomes the yield stress, while those predicted by the Bingham fluid model reduce to them in those regions. The corresponding viscosity values are found to be in agreement with the values measured using a parallel-plate viscometer. However, near the inclined wedge surface the yield stress dominates and creates a domain with a plug flow typical of the yield-stress materials, as predicted by the Bingham model. Two types of core formation, attached and floating, were visualized in the present experiments.

Carbopol gels exhibit pseudoplastic power-law fluid behavior in simple shear flows, as well as possess a yield stress revealed by squeeze flows. The general flow structure in the wedge-like flow can be characterized using a Newtonian fluid model in domains of high shear near the moving surface, albeit the Bingham fluid model must be used in lower shear domains. The latter reveals the characteristic reverse flow zone containing a rigid core, which is confirmed in the experiments with Carbopol solutions.

The agreement of the viscosity values measured in the wedge-like flow experiments based on the Newtonian fluid model with the one measured in the simple shear flow at the shear rate corresponding to the shear rate near the entrance of the wedge-like gap is quite remarkable. Furthermore, in the domains of low shear it was found in the framework of the Bingham fluid model that the viscosity increases, as expected for a shear-thinning fluid. Overall, it appears that using both Newtonian and Bingham models in conjunction elucidates more information than only for a single model.

Note also that during the experiments, it was observed that trapped air bubbles would recirculate within the fluid and would periodically exit the front of the wedge-like gap.

Furthermore, air bubbles were formed at the contact line between the rolling edge at the back of the wedge and the moving surface. These bubbles would typically stay near the moving surface and exit the wedge. This deserves exploration in future.

ACKNOWLEDGEMENT

This work was partially supported by The US Gypsum Corporation (USG). The authors are grateful for support of N.K.'s work through NSF Grant #1062943. Some elements of her project incorporated in the present work were described in Klep et al. (2014).

References

- Balmforth, N. J., Frigaard, I. A., and Ovarlez, G., Yielding to stress: Recent developments in viscoplastic fluid mechanics. *Annu. Rev. Fluid Mech.*, 46, 121-146 (2014).
- Batra, R. L., Rheodynamic lubrication of a journal bearing, *Applied Scientific Research, Section A 15.1*, 331-344 (1966).
- Dorier, C., and Tichy, J.A., Behavior of a Bingham-like viscous fluid in lubrication flows, *Journal of Non-Newtonian Fluid Mechanics*, 45, 291-310 (1992).
- Frigaard, I. A., and Ryan, D. P., Flow of a visco-plastic fluid in a channel of slowly varying width. *Journal of Non-Newtonian Fluid Mechanics*, 123, 67-83 (2004).

- Klep, N., D. Pelot, and A.L. Yarin. Spreading of a Herschel-Bulkley fluid using lubrication approximation. *J. Undegrad. Res.*, 7, 10-14 (2014).
- Loitsyanskii, L.G. *Mechanics of Liquids and Gases*. Oxford: Pergamon, 1966; Loitsyanskii, L.G. *Mechanics of Liquids and Gases*. New York: Begell House, 1996.
- Milne, A. A., A theory of rheodynamic lubrication and wear division, *Colloid & Polymer Science* 139.1, 96-101 (1954).
- Pelot, D. D., Sahu, R. P., Sinha-Ray, S., and Yarin, A.L. Strong squeeze flows of yield-stress fluids: The effect of normal deviatoric stresses, *Journal of Rheology*, 57, 719-742 (2013).
- Putz, A., Frigaard, I. A., and Martinez, D. M., On the lubrication paradox and the use of regularisation methods for lubrication flows. *Journal of Non-Newtonian Fluid Mechanics*, 163, 62-77 (2009).
- Schlichting, H., *Boundary-Layer Theory*. McGraw Hill, New York, 7th ed. 1987.
- Schramm, H. *A Practical Approach to Rheology and Rheometry*. Gebrueder HAAKE GmbH, Karlsruhe, 2nd. ed. 2000.
- Szabo, P., and Hassager, O., Flow of viscoplastic fluids in eccentric annular geometries. *Journal of Non-Newtonian Fluid Mechanics*, 45, 149-169 (1992).
- Tadmor, Z., and Gogos, C.G., *Principles of Polymer Science*. Wiley, 2006.
- te Nijenhuis, K. Section 9.1.2 Rheogoniometers and rheometers, in *Springer Handbook of Experimental Fluid Mechanics* (Eds. C. Tropea, A.L. Yarin, J. Foss), Springer, Heidelberg, 2007.
- Tichy, J. A., Hydrodynamic lubrication theory for the Bingham plastic flow model, *Journal of Rheology*, 35, 477-496 (1991).

Wada, S., Hayashi, H., and Haga, K. Behavior of a Bingham Solid in hydrodynamic lubrication:

Part 1, General theory, Bulletin of JSME, 16, 422-431 (1973).

Weinstein, S. J., and Ruschak, K.J., Coating flows, Annu. Rev. Fluid Mech, 36, 29-53 (2004).